Permeability of open-cell foams under compressive strain

M.A. Dawson [a,*], J.T. Germaine [b], L.J. Gibson [c]

[a] *Department of Mechanical Engineering, Massachusetts Institute of Technology, Cambridge, MA 02139, USA*
[b] *Department of Civil and Environmental Engineering, Massachusetts Institute of Technology, Cambridge, MA 02139, USA*
[c] *Department of Materials Science and Engineering, Massachusetts Institute of Technology, Cambridge, MA 02139, USA*

Abstract

A model for the behavior of low-density, open-cell foam under compressive strain is proposed. Using this model, a tractable relationship between the normalized permeability and the applied strain is developed. An experimental study of the effect of strain on the permeability of open-cell polyurethane foams is presented. The experiments are performed using a Newtonian fluid in the fully laminar regime, where viscous forces are assumed to dominate. The model is found to describe the experimental data well and be independent of the foam cell size, the direction of flow with respect to the foam rise direction, and the properties of the saturating fluid. In a companion paper, the model for the permeability of open-cell foam is combined with Darcy's law to give the contribution of viscous fluid flow to the stress–strain response of a reticulated foam under dynamic loading.
Published by Elsevier Ltd.

Keywords: Open-cell foam; Porous; Permeability; Strain; Deformation

1. Introduction

1.1. Background

The enormous pressure gradients generated by explosive devices can be harmful to the human body, as well as vehicles and structures. Existing armor is ineffective at reducing this pressure gradient. Recently, a novel approach to solving this problem has been proposed by incorporating open-cell (reticulated) foams filled with shear thickening, non-Newtonian liquids into existing composite armor. Open-cell foams filled with shear thickening liquids have the potential to impede shockwaves, increasing the time it takes waves to propagate through the foam medium and decreasing the resulting pressure gradient experienced by subsequent media. The flow of fluids through open-cell foams has been investigated extensively for a variety of engineering applications, but understanding and characterizing the contribution of the fluid to energy absorption under

* Corresponding author. Tel.: +1 617 253 5299; fax: +1 617 258 6275.
  E-mail address: dawson@mit.edu (M.A. Dawson).

dynamic loading is still a critical area of research. Previous research has resulted in the development of complex models to describe the contribution of Newtonian fluids in open-cell foams under impact loading. Hilyard (1971) provided one of the first in-depth analytical and experimental analyses of the contribution of fluid flow to the impact behavior of open-cell foams, developing a third order, non-linear equation of motion. Rehkopf et al. (1996), Mills and Lyn (2002), and Schraad and Harlow (2006) all developed finite difference and finite volume techniques to analyze the contribution of the fluid flow in an open-cell foam under dynamic loading. However, the inherent complexity of these models has limited their use. Here, to develop a more tractable model, we explore the intrinsic permeability of a liquid-filled, open-cell foam under compressive strain. In a companion paper, this model for foam permeability is combined with Darcy's law to obtain the contribution of the liquid to the stress–strain response of the foam.

Gent and Rusch (1966) studied the intrinsic permeability of open-cell foams. They first demonstrated that the average cell diameter is a function of the applied compressive strain, and proposed a qualitative, empirically based relation between the strain and the average cell diameter. They developed a simple model to determine the flow regime in an open-cell foam, modeling it as an array of smooth tubes. The theoretical transition from the fully laminar regime, where Darcy's law is applicable, to the inertial dominated regime should occur for $Re > 2000$ in a smooth walled tube. However, experimentally, they found the transition in open-cell foams from viscous to inertial dominated flow occurred for $Re \cong 1$, which also corresponded with the experimental findings of Tek (1957) for flow through porous rock and Dybbs and Edwards (1984) for fixed beds of spheres and cylinders. In all of these cases, the flow path is more tortuous than the case of flow through a smooth tube. Comiti et al. (2000) developed a model for this transition analytically, proposing a theoretical transition value of $Re = 0.83 \cong 1$ for flow through porous media.

Hilyard and Collier (1987) extended Gent and Rusch's work, developing and testing a theoretical model for predicting the effect of strain on permeability of a reticulated polyurethane foam. However, their experiments focused on air flow through foams with relatively large cell sizes. For all of their experiments $Re > 1$, so the effect of inertial forces could not be neglected. The flow of shear thickening fluids through open-cell foams under compressive loads is laminar and dominated by viscous forces for nearly all achievable strain rates. Neither Gent and Rusch (1966) nor Hilyard and Collier (1987) studied this flow regime in depth.

In this paper an improved relation between the permeability and compressive strain of an open-cell foam filled with a Newtonian liquid is developed. Both the cells that remain linear-elastic and those that collapse during compression are modeled. An experimental study of the effect of strain on the permeability of open-cell polyurethane foams is presented. The experimental results are used to determine the single empirical constant for the model. The experiments are performed using water in the fully laminar regime, which is readily extended to the study of the flow of shear thickening fluids in open-cell foams. The model is found to describe the experimental data well and be independent of the foam cell size, the direction of flow with respect to the foam rise direction, and the properties of the saturating fluid. The companion paper couples this relation with Darcy's law to give an equation for the contribution of the flow of a Newtonian fluid to the stress–strain response of an open-cell foam under dynamic loading.

1.2. Permeability model

Assuming the foam can be described as isotropic, the relative density under uniaxial compression, where the strain ε, is taken to be negative in compression, is given as

$$\frac{\rho^*}{\rho_s} = \frac{\rho_o^*}{\rho_s} \frac{1}{(1 + \varepsilon)(1 - v\varepsilon)^2} \tag{1}$$

where ρ_o^* is the initial density of the foam at 0% compression, ρ^* is the density of the foam at strain ε, ρ_s is the density of the solid from which the foam is made, and v is Poisson's ratio of the foam. For compressive strains above about 7.5%, the cells in open-cell flexible foams buckle and collapse without expanding laterally, so that their Poisson's ratio in this regime is approximately zero. Since the focus of this analysis is primarily in the behavior at high strains, $v\varepsilon$ is taken to be zero for low-density, open-cell, flexible foams. Substituting Eq.

(1) into the porosity term of Brace's equation for porous media, the intrinsic permeability k, of the foam is given by (after Brace, 1977)

$$k = Ad^2 \left(1 - \frac{\rho_o^*}{\rho_s} \frac{1}{(1+\varepsilon)} \right)^3 \tag{2}$$

where A is an empirical constant and d is the average diameter of the cells.

As the foam is compressed beyond the elastic buckling strain ε_{el}^* of 7.5%, layers of cells buckle and collapse, generating local bands of large deformation in which the average diameter of the cells is reduced substantially. A detailed discussion of this banding phenomenon, which is widely seen in open-cell polymeric foams, is given by Gioia et al. (2000). As the initial collapse band forms, the rest of the specimen remains in the linear elastic regime, at a strain close to the elastic buckling strain, ε_{el}^*. As the overall strain increases, cells adjacent to the collapsed band also collapse, so that the length of the densified band increases while that of the remainder of the foam in the linear elastic regime decreases. The strain of the collapsed cells in these densified bands is assumed to be uniform and given by the densified strain ε_d (Fig. 1). Fig. 2 demonstrates the existence of the two regimes in reticulated polyurethane foam with an approximate relative density of 3% under a compressive strain of 0.4. Fig. 3 shows magnified images of the collapsed cells for compressive strains ranging from 0.2 to 0.8. The collapsed cells at strains of less than or equal to 0.6 are of comparable size while at higher strains, cells begin to densify further. Therefore, the densified strain is taken to be $\varepsilon_d = 0.6$ for all grades of reticulated polyurethane foams with approximate relative density of 3%. This corresponds well with Hilyard and Collier (1987) who proposed the compaction of cells invalidates any relations between the average cell size and the strain beyond compressive strains of 60%. We focus our model at strains less than 60%.

Gent and Rusch (1966) consider the foam to be modeled as an array of circular tubes. The average diameter of a cell, given to be proportional to the ratio of the volume of a tube to the wetted surface area of a tube, is found to be proportional to the diameter of the cross-section of the tube. For a small uni-directional compressive deformation of low-density foam, they assume the cross-section of the flow channels deforms in the same proportion as the bulk material. Using a small strain approximation, they give the average diameter of a cell under 1-dimensional compressive strain in the elastic regime by

$$d_{el} \cong d_o(1+\varepsilon)^{1/2} \quad \text{for } 0 \leqslant \varepsilon \leqslant \varepsilon_{el}^* \tag{3}$$

where d_o is the average cell size at 0% strain. We further propose the average diameter of a cell in the densified regime d_d follows a similar form and is given as
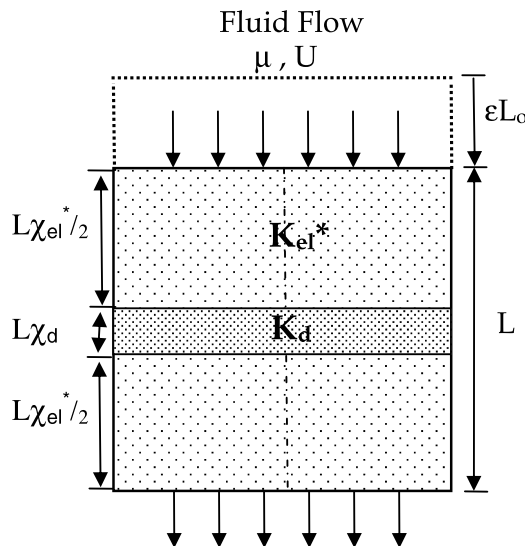

Fig. 1. Model of fluid-filled cylindrical foam specimen compressed beyond elastic buckling strain, ε_{el}^*.
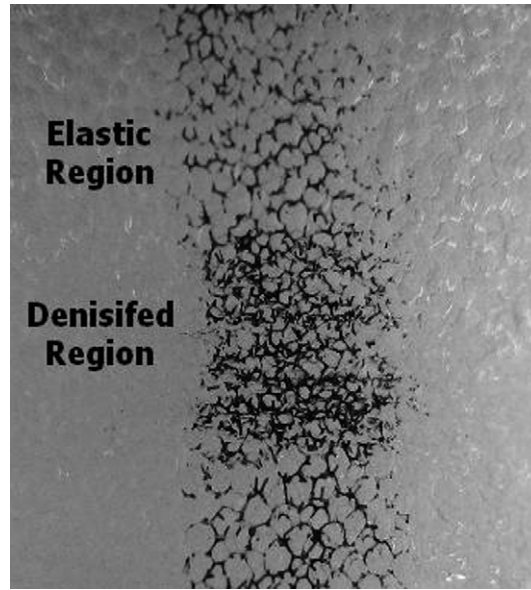
Fig. 2. Compression of a saturated, 90 ppi, polyurethane foam specimen at 40% strain.
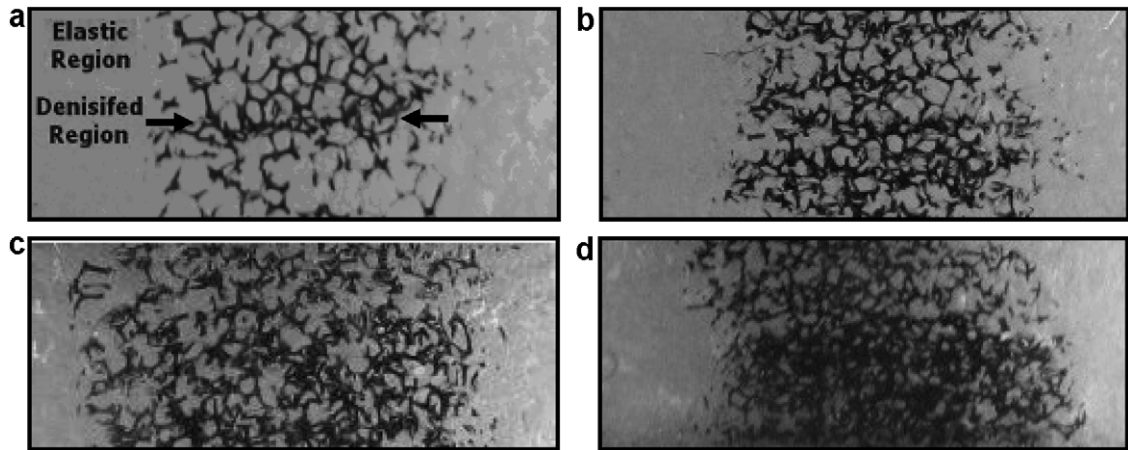

Fig. 3. Magnified compression laps photos of densified region for a saturated, 90 ppi, polyurethane foam specimen. (a) 20% strain, (b) 40% strain, (c) 60% strain, (d) 80% strain.

$$d_{\mathrm{d}} = d_{\mathrm{o}}(1+\varepsilon)^{a} \quad \text{for } \varepsilon = \varepsilon_{\mathrm{d}} \tag{4}$$

where a is an empirical constant. The corresponding permeabilities in the linear elastic regime k_{el}, in the elastic buckling regime k_{el}^{*}, and in the densified regime k_{d}, are determined by coupling Eqs. (2)–(4) and given by

$$k_{\mathrm{el}} = A d_{\mathrm{o}}^{2}(1+\varepsilon)\left(1 - \frac{\rho_{\mathrm{o}}^{*}}{\rho_{\mathrm{s}}}\frac{1}{(1+\varepsilon)}\right)^{3} \quad \text{for } 0 \leqslant \varepsilon \leqslant \varepsilon_{\mathrm{el}}^{*} \tag{5}$$

$$k_{\mathrm{el}}^{*} = A d_{\mathrm{o}}^{2}(1+\varepsilon_{\mathrm{el}}^{*})\left(1 - \frac{\rho_{\mathrm{o}}^{*}}{\rho_{\mathrm{s}}}\frac{1}{(1+\varepsilon_{\mathrm{el}}^{*})}\right)^{3} \quad \text{for } \varepsilon = \varepsilon_{\mathrm{el}}^{*} \tag{6}$$

$$k_{\mathrm{d}} = A d_{\mathrm{o}}^{2}(1+\varepsilon_{\mathrm{d}})^{2a}\left(1 - \frac{\rho_{\mathrm{o}}^{*}}{\rho_{\mathrm{s}}}\frac{1}{(1+\varepsilon_{\mathrm{d}})}\right)^{3} \quad \text{for } \varepsilon = \varepsilon_{\mathrm{d}} \tag{7}$$

Furthermore, the corresponding volume fractions of the cells remaining in the linear elastic regime χ_{el}^*, and the densified regime χ_d, after the onset of cell buckling, are given by

$$\chi_{el}^* = \frac{(\varepsilon_d - \varepsilon)(1 - \varepsilon_{el}^*)}{(1 - \varepsilon)(\varepsilon_d - \varepsilon_{el}^*)} \quad \text{for } \varepsilon_{el}^* \leqslant \varepsilon \leqslant \varepsilon_d \tag{8}$$

$$\chi_d = \frac{(\varepsilon - \varepsilon_{el}^*)(1 - \varepsilon_d)}{(1 - \varepsilon)(\varepsilon_d - \varepsilon_{el}^*)} \quad \text{for } \varepsilon_{el}^* \leqslant \varepsilon \leqslant \varepsilon_d \tag{9}$$

Gent and Rusch (1966) developed a model relating the total pressure drop Δp across a specimen to the fluid properties, foam properties, and flow velocity U:

$$\frac{\Delta p}{L} = \frac{\mu}{k_T} U + \frac{\rho}{B_T} U^2 \tag{10}$$

where L is the length of the specimen in the direction of flow, μ is the dynamic viscosity of the fluid, ρ is the density of the fluid, k_T is the effective permeability of the foam, and B_T is the inertial flow coefficient of the foam. The inertial flow coefficient has the dimensions of length and is characteristic of the geometry of the media, the cell size, and the nature of the flow. They attributed the first term on the right-hand side of the equation to viscous forces, corresponding to Darcy's law governing laminar flow, and the second term to inertial forces dominant in the turbulent regime. The flow of shear thickening fluids in open-cell foams is dominated by viscous forces for nearly all achievable strain rates. Therefore, the focus of this paper is the fully laminar regime dominated by viscous flow where the second term on the right-hand side of Eq. (10) can be neglected. Assuming the flow is laminar and dominated by viscous forces the pressure drop Δp_i across each regime of the foam is given by

$$\frac{\Delta p_i}{L_i} = \frac{\mu}{k_i} U \tag{11}$$

where L_i is the length of each regime in the direction of flow and k_i is the intrinsic permeability of each regime. The flow velocity U is assumed uniform and taken to be constant through each regime because of continuity. Combining Eqs. (10) and (11), noting the total pressure drop across the specimen is equal to the sum of the pressure drops across each regime, and noting that the length of each regime is proportional to the volume fraction of each regime, the effective permeability as a function of strain is given by

$$k_T = k_{el} \quad \text{for } 0 \leqslant \varepsilon \leqslant \varepsilon_{el}^* \tag{12}$$

$$k_T = \frac{k_d k_{el}^*}{\chi_{el}^* k_d + \chi_d k_{el}^*} \quad \text{for } \varepsilon_{el}^* \leqslant \varepsilon \leqslant \varepsilon_d \tag{13}$$

Coupling the previous relations for low-density foam the normalized intrinsic permeability k_T/k_O can be approximated as

$$\frac{k_T}{k_o} \cong (1 + \varepsilon) \quad \text{for } 0 \leqslant \varepsilon \leqslant \varepsilon_{el}^* \tag{14}$$

$$\frac{k_T}{k_o} \cong \frac{(1 + \varepsilon_d)^{2a}(1 + \varepsilon_{el}^*)}{\chi_{el}^*(1 + \varepsilon_d)^{2a} + \chi_d(1 + \varepsilon_{el}^*)} \quad \text{for } \varepsilon_{el}^* \leqslant \varepsilon \leqslant \varepsilon_d \tag{15}$$

where k_o is the permeability at 0% strain.

2. Materials and methods

2.1. Materials

Specimens of open-cell, flexible, polyester-based polyurethane foams (Foamex, Linwood, PA), with nominal cell diameters of 175, 210, and 235 μm based on manufacturers specifications (corresponding to grades of 90, 80, and 70 pores per inch (ppi), respectively) were used in the tests. The densities of the foams ranged from

0.0318 to 0.0322 g/cm^3. The relative density of the foams was taken to be $\rho^*/\rho_s \cong 0.03$, based on the manu-facturer's value of the density of the solid polyurethane ($\rho_s = 1.078$ g/cm^3). The foam was cut into uniform cylindrical specimens of 36.0 mm diameter with heights ranging from 32 to 34 mm. The dimensions of each sample were measured using a digital caliper accurate to within 0.01 mm. The mass of each sample was mea-sured using an electronic balance accurate to 0.1 g (PB3002, Mettler Toledo, Switzerland).

2.2. Experimental procedure

The permeability of each specimen was measured for compressive strains ranging from 0% to 60%, in incre-ments of 5% and at the elastic buckling strain of 7.5%. Prior to testing, each sample was fully saturated under a vacuum of 762 mm of mercury to ensure that every pore was completely filled with water, the working fluid. After saturation, the foam samples remained submerged in water for the duration of the experiment. Water was driven through the specimen using gravity-driven flow between two adjustable reservoirs, which stabilize the flow (Fig. 4).

The specimen was contained in a cylindrical glass tube with an inner diameter of 35.8 mm. The inlet and outlet of the tube were sealed with rubber stoppers equipped with pressure taps, allowing for measurement of the pressure drop across the foam specimen using a manometer and a traveling microscope which read to the nearest 0.0254 mm (Titan Tool Supply Co, Buffalo, NY). The pressure drop was measured across the cylindrical glass tube and compression device alone (i.e. without the foam specimen) and found to be neg-ligible for all flow rates used in this experiment. The flow rate was determined by measuring the mass of the water exiting the second reservoir over a specified period of time. The velocity of the fluid entering the spec-imen was found from the flow rate and the cross-sectional area of the glass tube, assuming the velocity distri-bution through the specimen was uniform. The sample time for each experiment was selected to be 90 s to ensure high accuracy. At each strain, six flow rates between 0.7 and 2.0 cm^3/s were selected and the corre-sponding pressure drop was measured. The temperature of the water in the system was maintained at 25.0 °C and continuously monitored at the inlet and exit reservoirs using digital thermometers. The viscosity of water at 25.0 °C is 8.9×10^{-4} Pa s.

The foam within the cylindrical glass tube was compressed using mesh "platens" that were screwed together as shown in Fig. 5 to impose increasing strain; the mesh has less than 1% cross-sectional interference with the specimens. The specimens were compressed axially, parallel to the direction of fluid flow. The glass tube had an inner diameter of 35.8 mm, giving negligible cross-sectional interference when the foam was uncompressed. However, the cross-sectional interference was sufficient to prevent flow around the foam specimen.

As previously discussed, the specimens do not significantly expand radially for the range of compressive strains used in these tests, so that the cross-sectional interference of the foam with the glass tube remains neg-ligible. The large strains used in these tests could result in some microstructural damage to the specimen. To
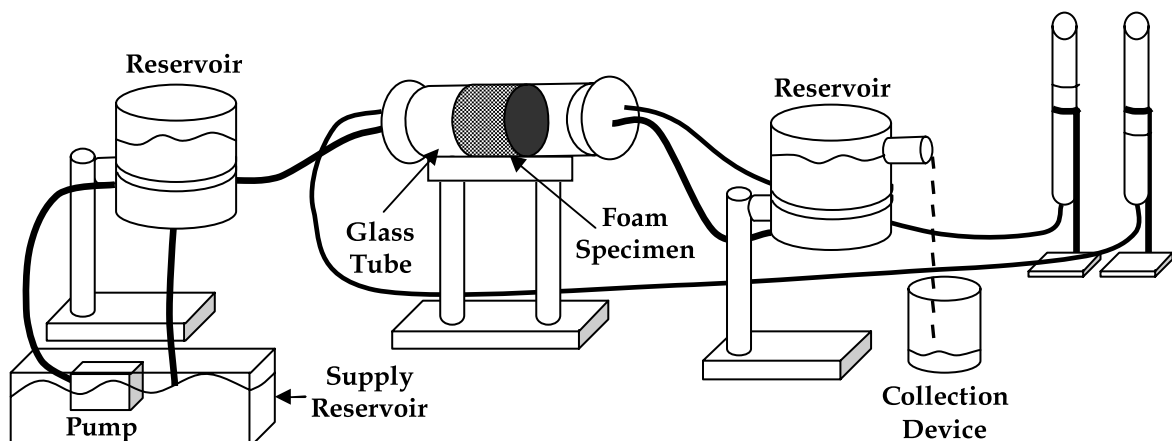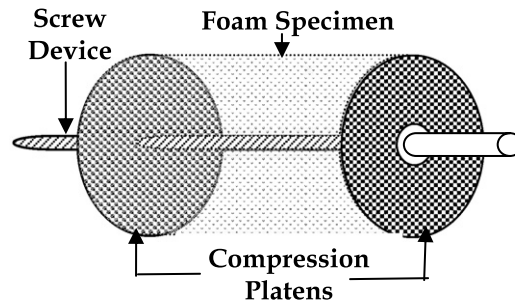

Fig. 4. Schematic for experimental setup.

Fig. 5. Foam compression device.

ensure the specimens are as uniform and similar as possible, each specimen was precompressed to 75% strain once prior to testing.

To satisfy Darcy's law for laminar flow and neglect the inertial term in Eq. (2), all of the experiments were conducted with $Re < 1$. For instance, the maximum Reynolds number in the experiments was found to be 0.53, corresponding to a velocity of 2×10^{-3} m/s in a 70 ppi foam with average cell diameter of 235 μm. For a maximum velocity of 2×10^{-3} m/s, the viscous term in Eq. (2) is two orders of magnitude larger than the inertial term, so that the inertial term can be neglected and the permeability can readily be determined from the slope of a plot of the pressure drop vs. the flow rate.

Nearly all prior experimental studies of permeability of an open-cell foam use air as the working fluid. In this experiment water is used, which is a highly polar fluid, known to have an effect on the properties of the solid polyurethane. In order to ensure these effects do not bias or invalidate the results, the effects of polar fluids on polyurethane foam were examined. Uniaxial compression tests of foam specimens were performed using a Texture Analyzer (TA XT Plus, Stable Microsystems, Hamilton, MA). The data acquisition system used was the Texture Exponent 32 code, which acquires both loading and positioning information for each test at a rate of 1 sample per second. The specimen was precompressed to 75% strain twice prior to testing. Based on Shen et al. (2001) the difference in the stress plateau between the 3rd, 4th, and 5th compressions should be negligible. The specimen was allowed to fully recover 24 h between compression tests. The specimens were loaded to 60% strain at a strain rate of 1×10^{-3} s^{-1}, which is assumed to be static so the contribution of the fluid flow to the strength and stiffness of the foam was taken to be negligible. Fig. 10 plots stress vs. strain curve for an 80 ppi foam under uniaxial compression before saturation with the polar fluid, during saturation with the polar fluid, and after removal of the polar fluid. The time degradation effects of saturating the foam with a polar fluid were also examined. Fig. 11 shows the stress–strain curves for a foam specimen saturated with water over a 72 h period. The curves are for a specimen compressed to 60% at a strain rate of 1×10^{-3} s^{-1}.

3. Results

3.1. Permeability vs. strain relation

A typical curve of the pressure drop vs. flow rate for an 80 ppi foam specimen with strains from 0% to 60% is given in Fig. 6. The coefficients of determination for these regressions were all above $R^2 = 0.99$. The permeability was determined from the slope of each of these regressions at the corresponding strain, ranging from 0% to 60%. The small deviation of each regression from the origin is neglected and can be attributed to small air bubbles trapped in the pressure taps and the effect of surface tension in the manometer readings. These experiments were repeated with three different specimens for each of the three types of foams. The permeability measurements were highly repeatable with all data points falling within 15% of the average value. The permeability of the specimens measured at 0% strain, given the symbol k_o, determined before and after precompression of each specimen is given in Table 1. Experimental data for the normalized permeability k_T/k_o is plotted against the strain ε in Fig. 7a–c. The solid regression line represents the model presented
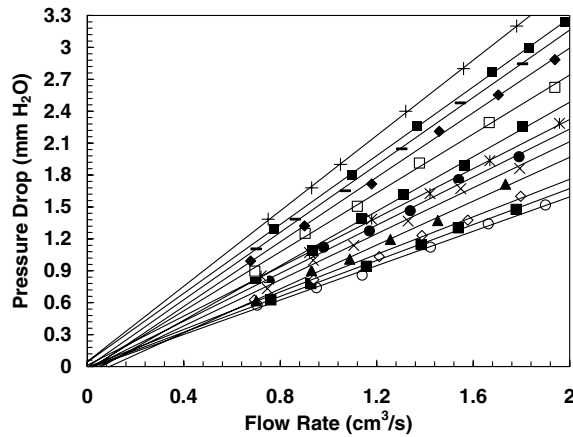
Fig. 6. A typical plot of pressure drop vs. flow rate for an 80 ppi specimen. Each regression line corresponds to a different strain varying from 0% (○) to 60% (+). The slope of each line increases correspondingly with increasing strain.

Table 1
Data for each grade of foam

Foam type (ppi)	Avg. cell dia. (μm)	Before precompression k_o ($1 \times 10^{-9}\,\mathrm{m}^{-2}$)	After precompression k_o ($1 \times 10^{-9}\,\mathrm{m}^{-2}$)	k_{el}^*/k_o	k_d/k_o	a
70 ∥	235	4.85	5.62	0.893	0.221	0.75
70 ⊥	235	4.67	5.02	0.902	0.214	0.76
80 ∥	210	3.70	3.68	0.897	0.198	0.80
90 ∥	175	3.24	4.98	0.900	0.181	0.85

The permeability at 0% strain for each grade of foam before and after precompression.. The coefficient a is the best-fit exponent which satisfies Eq. (8). ⊥ and ∥ correspond to the direction of flow being perpendicular and parallel to the rise direction, respectively.

by Eqs. (12) and (13) where the coefficient a, is fitted to satisfy k_d. The best-fit coefficient a, for each grade of foam is given in Table 1. The broken regression lines are representative of the data found by Gent and Rusch (1966) and Hilyard and Collier (1987) for low density foams. The data are found to be well approximated by the following regression equations:

$$\text{Gent and Rusch Data}\quad \frac{k_{\mathrm{T}}}{k_o} \cong (1+\varepsilon)^{1.8} \quad \text{for } 0 \leqslant \varepsilon \leqslant \varepsilon_d \tag{16}$$

$$\text{Hilyard and Collier Data}\quad \frac{k_{\mathrm{T}}}{k_o} \cong (1+\varepsilon)^{2.2} \quad \text{for } 0 \leqslant \varepsilon \leqslant \varepsilon_d \tag{17}$$

Fig. 8 is included to compare the model presented in this analysis for the normalized permeability to the models presented by Gent and Rusch (1966) and Hilyard and Collier (1987). The Gent and Rusch (1966) model is the same as the relation found in Eq. (14). The Hilyard and Collier (1987) model, which is based on empirical relations for low-porosity foam, is slightly more complex, containing non-linear functions of the porosity and strain. The data plotted in Fig. 8 corresponds to the data in Fig. 7b for 70 ppi polyurethane foam. It is clear the model presented in this analysis improves upon the Gent and Rush model and provides a similar fit to the Hilyard and Collier model.

The low-density foams in this experiment are anisotropic with cell lengths in the rise direction approximately 1.8 times larger than those in the plane perpendicular to the rise direction. Experiments were performed with the fluid running both parallel and perpendicular to the rise direction with strain applied in the direction of fluid flow. The permeability at 0% strain for the 70 ppi specimens when the flow is parallel to the rise direction of the foam is found to be nearly the same as when the flow is perpendicular to the rise direction as shown in
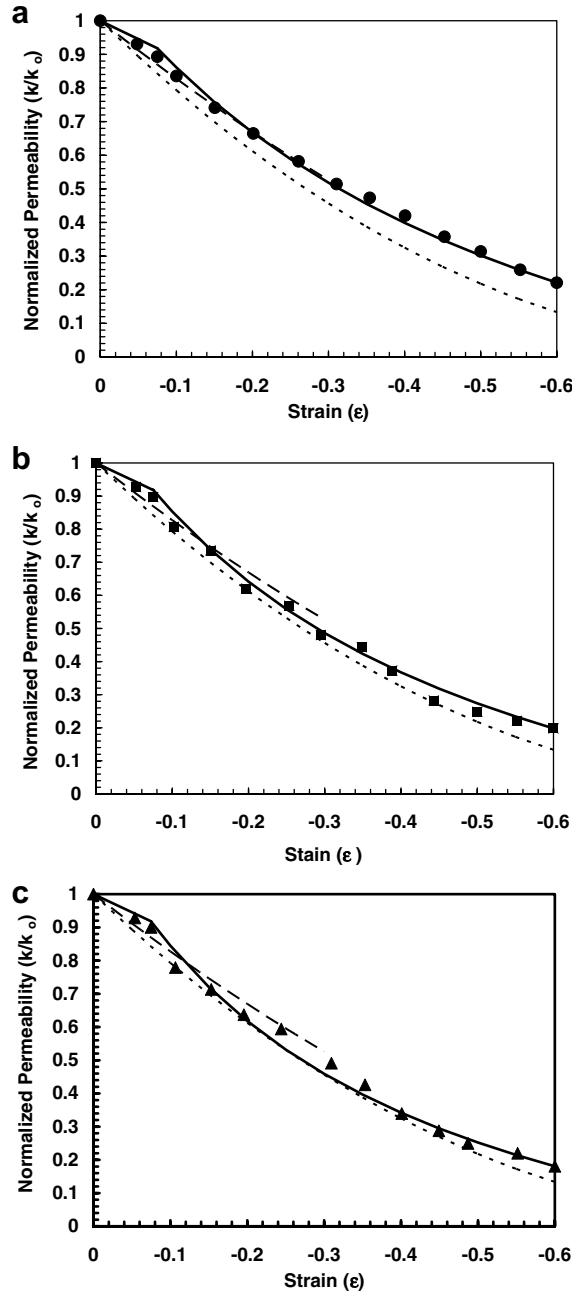
Fig. 7. (a) The normalized permeability k/k_o plotted vs. strain ε for 70 ppi polyurethane foam. (b) The normalized permeability k/k_o plotted vs. strain ε for 80 ppi polyurethane foam. (c) The normalized permeability k/k_o plotted vs. strain ε for 90 ppi polyurethane foam. Gent and Rusch regression (- - -), Hilyard and Collier regression ($\cdots\cdots$), Dawson, Germaine, and Gibson Model (—).

Table 1. A sample plot of the normalized permeability plotted vs. strain for 70 ppi foam with fluid flowing both perpendicular and parallel to the rise direction of the foam is given in Fig. 9. Fig. 9 demonstrates that the relationships between the normalized permeability and the strain for the flow parallel or perpendicular to the rise direction of the foam are nearly identical.
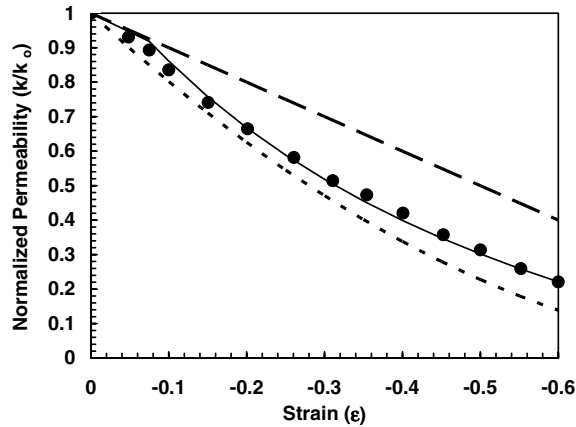
Fig. 8. The normalized permeability k/k_o plotted vs. strain ε for the Gent and Rusch model (- - -), Hilyard and Collier model (· · · · · ·), and Dawson, Germaine, and Gibson Model (—) against data for 70 ppi polyurethane foam.
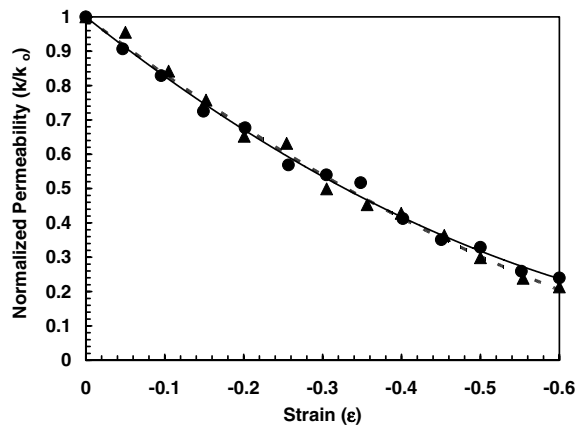

Fig. 9. Flow orientation independence. The normalized permeability k/k_o plotted vs. strain ε for grade 70 ppi polyurethane foam. Direction of flow is perpendicular (- -▲- -), parallel (–•–) to the rise direction.

3.2. Effect of polar fluid on model

Fig. 10 verifies the previously established results that saturating a polyurethane foam with a polar fluid reduces the stiffness and strength. Once the polar fluid is removed and the foam is completely dried, the stress–strain response of the foam is nearly restored. Fig. 11 shows the plateau stress and modulus remain approximately constant over the time frame utilized for these experiments. Both Figs. 10 and 11 are plotted through 30% strain to provide higher resolution of the linear elastic regime and plateau stress. The plateau stress and modulus remain approximately constant over the duration of the time frame considered.

4. Discussion

The permeability of each specimen measured before precompression is consistent with the range of expected values previously reported by the manufacturer (Foamex, Linwood, PA) and follows the expected trend with average cell size; permeability decreases with decreasing pore size. However, the permeability at 0% strain after precompression is not consistent with the expected trend. This phenomenon is also observed in Hilyard and Collier's (1987) study. Their data show after mechanically conditioning (i.e. precompressing) the foam, the permeability was changed dramatically and the normal trend relating the permeability to the average cell size
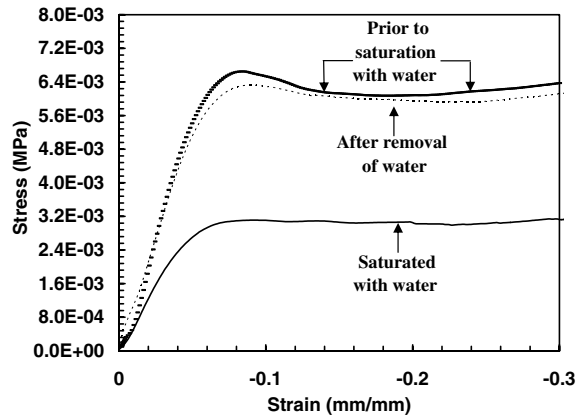
Fig. 10. Fluid degradation effect. Stress plotted vs. strain for an 80 ppi foam. (- - -) Prior to saturation with water, (—) saturated with water, (· · · · · ·) after removal of water.
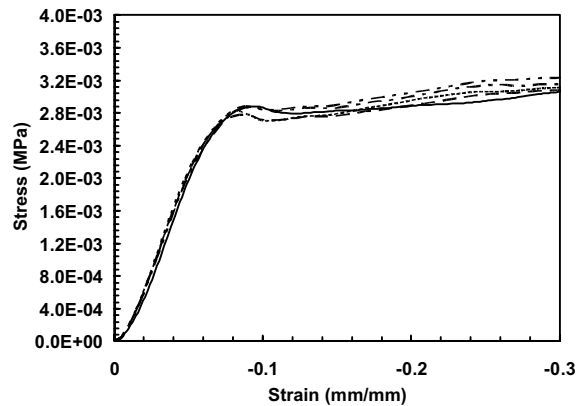

Fig. 11. Fluid degradation effect with time. Stress plotted vs. strain for an 80 ppi foam saturated with water over time t. —, $t = 0$ h; - - -, $t = 12$ h; – –, $t = 24$ h, -··-·, $t = 48$ h, –··, $t = 72$ h.

was no longer valid. In addition, the effect of saturating the foam with a polar fluid, may have affected the microstructure of each grade of foam differently, making one grade of foam disproportionately more compliant and more permeable than another.

The solid regression lines, representing the model for the normalized permeability as a function of strain, given by Eq. (12) and (13), describe the data in Fig. 7a–c well. The normalized permeability at the elastic buckling strain $k_{\mathrm{el}}^*/k_{\mathrm{o}}$, is nearly constant for all three grades of foam (Table 1), deviating on average from the elastic model given by Eq. (12) by approximately 2%. The normalized permeability at the densified strain $k_{\mathrm{d}}/k_{\mathrm{o}}$, differs slightly for all three grades of foams, giving distinctly different values for the best-fit coefficients a. However, averaging the coefficients for all three grades of foams, giving $a = 0.80$, provides a reasonable model which fits the data well for all three foam grades.

In addition, this average model corresponds well with previously reported experimental results given by Gent and Rusch (1966) and Hilyard and Collier (1987). The range of cell sizes examined in these studies was up to an order of magnitude larger than those presented here, indicating the relation between the normalized permeability and the strain is independent of the cell size of the foam. Therefore, the model presented in Eqs. (14) and (15) with coefficient $a = 0.80$ is taken to be applicable to all cell sizes of low relative density foam.

Fig. 8 compares the model presented in this analysis to the models given by Gent and Rusch (1966) and Hilyard and Collier (1987) for an 70 ppi polyurethane foam. The model presented in this analysis is found to improve significantly upon the model given by Gent and Rush and provide a similar fit to the Hilyard

and Collier model. However, the model developed in this paper provides a more physically based description of the behavior of the foam under compression. This allows for the model to be readily extended to more complex analyses such as analyzing the contribution of fluid flow to the stress–strain response of foam under dynamic compression as presented in a companion paper.

Moreover, this model is also observed to be independent of whether the orientation of the rise direction of the foam is perpendicular or parallel to the direction of fluid flow. Fig. 9 shows a negligible difference in the best fit relation between the permeability and the strain for the two flow directions. Therefore, the relations given in Eqs. (14) and (15) are taken to be independent of whether the rise direction of the foam is parallel or perpendicular to the fluid flow direction.

Furthermore, to ensure the model is independent of the saturating fluid, the effects of saturating the foam with a polar fluid were also examined. Fig. 10 verifies the previously established results that saturating a polyurethane foam with a polar fluid immediately reduces its stiffness and strength. The polar fluid acts to weaken the microstructure of the foam by interfering with the hydrogen bonding, resulting in a decrease in the modulus of the solid polyurethane. Once the polar fluid is removed and the foam is completely dried, the stiffness of the foam is nearly restored. This is expected since the interference of the polar fluid with the hydrogen bonding of the polymer chains is removed. This corresponds well with the theory of Hogan et al. (1973); once water molecules are completely removed from the foam, hydrogen bonds in the polymer reform, and the original strength of the foam is restored. The slightly lower plateau stress in Fig. 10 indicates the polar fluid allows for more rapid microstructural degradation during loading than a dry foam experiences. The buckling strain of the saturated foams also indicates microstructural changes to the foam are more readily caused by loading a foam where the hydrogen bonds are weakened by a polar fluid. Unlike the modulus and maximum buckling stress, which depend on the material properties, the buckling strain is completely dependent on the microstructure. The buckling strain of the foam saturated with water is slightly lower than that of the dry, unsaturated foam, indicating minute microstructural damage. Although saturation of a foam with a polar fluid weakens the bonding and allows for deformation to more readily damage the microstructure, the minor additional deformation due to a polar fluid should not alter the permeability significantly from the permeability measured with a non-polar fluid.

In addition, in Fig. 11 the plateau stress and modulus remain approximately constant, demonstrating saturating a polyurethane foam with a polar fluid does not degrade the microstructure over the time frame considered. Hogan et al. (1973) shows similar findings that the effect of relative humidity on the time degradation of polyurethane foam is negligible over the time frame considered in this study. Therefore, neglecting the effect of the polar fluid on the permeability of the foam specimens is valid, and the proposed relations given in Eq. (14) and (15) are found to be independent of the saturating fluid.

5. Conclusion

In this paper, a study of the effect of strain on the permeability of reticulated polyurethane foam saturated with a polar fluid in the laminar regime is performed. Using the fact that the permeability is a function of the applied compressive strain, a physically based composite model, based on the permeability of the linear elastic regime and that of the densified regime, is developed. This relation is found to be independent of the cell size of the foam, the direction of flow relative to the foam rise direction, and the saturating fluid. This relation is extended in a companion paper to give a tractable model for the contribution of viscous fluid flow in an open-cell foam under dynamic loading. Future work will focus on validating the model for the stress–strain response of an open-cell foam filled with Newtonian fluid experimentally and extending the analysis to account for the effects of non-Newtonian fluid flow through reticulated media. Developing an improved understanding of the contribution of a non-Newtonian liquid to energy absorption under dynamic loading is critical to the successful development of fluid-filled foams capable of impeding shockwaves.

Acknowledgements

References

Brace, W., 1977. Permeability from resistivity and pore shape. J. Geophys. Res. (82), 3343–3349.

Comiti, J. et al., 2000. Experimental characterization of flow regimes in various porous media-III: limit of Darcy's or creeping flow regime for newtonian and purely viscous non-newtonian fluids. Chem. Eng. Sci. (55), 3057–3061.

Dybbs, A., Edwards, R.V., 1984. A new look at porous media fluid mechanics-Darcy to turbulent. In: Bear, J., Cor., Y. (Eds.), Fund. Trans. Phen. Martinus Nishoff, Dordrecht, pp. 199–256.

Gent, A., Rusch, K., 1966. Permeability of open-cell foamed materials. J. Cell. Plast., 46–51.

Gioia, G. et al., 2000. The energetics of heterogeneous deformation in open-cell solid foams. Proc. R. Soc. Lond. A. (457), 1079–1096.

Hilyard, N.C., 1971. Observations on the impact behaviour of polyurethane foams; II. The effect of fluid flow. J. Cell. Plast., 84–90.

Hilyard, N., Collier, P., 1987. A structural model air flow flexible pur foams. Cell. Polym. (6), 9–26.

Hogan, J. et al., 1973. Humidity characteristics HR hot urethane foams. J. Cell. Plast. (9), 219–225.

Mills, N., Lyn, G., 2002. Modeling air flow in impacted polyurethane foam. Cell. Poly. (21), 343–365.

Rehkopf, J., Brodland, G., McNeice, G., 1996. Experimentally separating fluid and matrix contributions to polymeric foam behavior. Exper. Mechan. (36), 1–6.

Schraad, M., Harlow, F., 2006. A multi-field approach to modeling the dynamic response of cellular materials. Int. J. Mech. Sci. (48), 85–106.

Shen, Y., Golnaraghi, F., Plumtree, A., 2001. Modeling compressive cyclic stress-strain behaviour of structural foam. Int. J. Fatigue (23), 491–497.

Tek, M., 1957. Development of a generalized darcy equation. J. Petro. Tech. 6 (9), 45–47.